CATALYZED HYDROGASIFICATION OF COAL CHARS

N. Gardner, E. Samuels, K. Wilks

INTRODUCTION

The reaction of hydrogen with coal and coal chars to produce gaseous hydrocarbons (hydrogasification) has received considerable attention for at least thirty-five years, since Dent in 1937 first reported on the hydrogasification synthesis[1]. The reaction proceeds in two steps. In the initial stage, reaction rates are extremely rapid as the volatile matter and more reactive components of the coal are hydrogenated. Subsequent rapid hydrogenolysis of the higher homologs formed yields methane. In the second stage of the reaction, the structure of the remaining carbon char is more graphitic in character, resulting in a much slower hydrogasification reaction. It is the catalysis of the slow, second stage of the hydrogasification reaction that we have initiated a study of at Case Western Reserve University.

There have been numerous reports and patents on the catalysis of a similar reaction--the liquid phase hydrogenation of coal to liquid and gaseous products. Hydrogenation reactions are generally carried out at high pressures (several hundred atmospheres) and low temperatures (400 to 500°C) where the hydrocarbon products formed are substantially liquid. The ability of tin-halogen compounds, alkali metals[2], and many other materials to catalyze the coal hydrogenation reactions is well known. Although the reaction is carried out in conditions where coal has undergone agglomeration and liquifaction,

the method of contacting catalyst and coal particles has a strong influence on reaction rate. For example, the addition of powdered ferrous sulfate to coal particles has almost no effect on the hydrogenation rate[3]. Impregnation of the coal by immersing it in aqueous solutions of ferrous sulfate, followed by oven drying, resulted in a sharp increase in hydrogenation rate with high productions of asphalt and oil. Impregnated nickelous chloride, stannous chloride, and ammonium molybdate show similar increases in catalytic activity as compared to powders of the same materials[4].

In contrast to hydrogenation reactions, for the hydrogasification of coal chars, much less is known about the catalytic activity of materials and the dependency of catalyst contacting techniques. Alkali carbonates, one to ten percent by weight, have been shown to catalyze the hydrogasification of coals and cokes at temperatures of 800-900°C[5]. The suggested mechanism was that adsorption of the alkalies by carbon prevented graphitization of the surface. Zinc and tin halides have been shown to be effective hydrogasification catalysts. There is, however, little kinetic information on any of the catalyzed hydrogasification reactions.

There have been extensive studies on the ability of particulate metals and metal salts to catalyze the reactions of graphitic carbon with oxygen and carbon dioxide. For example, colloidal iron on Ticonderoga graphite reduces the activation energy for the carbon-oxygen reaction from 46 kcal/mole to 10 kcal/mole. A seven percent iron deposit impregnated from solution on sugar char reduced the

activation energy from 61.2 kcal/mole to 22.8 kcal/mole for the carbon-carbon dioxide reaction. In addition, dispersions of metals in carbon have been prepared by carbonization of polymers containing metal salts. The dispersions are catalytically active in the gasification reactions of carbon dioxide and oxygen. The mechanism of the substantial reduction in activation energy is not clear although a large amount of superfluous, quantitative information has been obtained. Two types of mechanisms have been proposed, oxygen-transfer and electron-transfer. In the oxygen-transfer mechanism the catalyst is presumed to assist the dissociation of molecular oxygen to chemisorbed atomic oxygen which then reacts with the carbon surface. Electron-transfer mechanisms involve the π electrons of graphitic carbon and the vacant orbitals of the metal catalysts. The catalytic effect presumably results from the altered electronic structure of the surface carbon atoms.

In contrast to the wealth of information on catalyzed hydrogenation of coal, and the catalyzed oxidation reactions of carbon by oxygen and carbon dioxide, little is known about catalyzed hydrogasification reactions as to the ability of materials to serve as catalysts. Also little is known about the kinetics and mechanisms of these reactions. We have initiated a kinetic study of catalyzed hydrogasification reactions using a high temperature, high pressure, recording balance. A thermobalance is particularly useful in gas-solid reactions because the weight of relatively small solid samples can be continuously measured. Direct kinetic analysis of the weight loss curves are straightforward.

II. EQUIPMENT AND PROCEDURES

The high pressure thermobalance is very similar to the balance described by Feldkirchner and Johnson[6]. The thermobalance was designed to operate isothermally at temperatures up to 1000°C and at hydrogen pressures up to 2000 psi. Details of the balance are shown in Figure 1, and a schematic diagram of the system is shown in Figure 2.

The reactor tube was constructed of Haynes 25 superalloy. The mass transducer is a Statham, Model UC 3, attached to a balance arm (Micro-scale accessory UL 5) and has a full scale range of 6 grams.

The sample is lowered into the reaction zone by an electric motor driven windlass at a rate of about one inch per second. The position of the sample in the reactor is obtained by utilizing a potentiometric technique. A small ten turn potentiometer is coupled directly to the windlass. Temperatures in the reactor are measured by stainless steel encased chromel-alumel thermocouples, the closest one to the sample being located 1/4" below the sample. Hydrogen flow rates were controlled ± 5 percent over the range 10 to 40 SCF/hr. Gas analysis was obtained by splitting a portion of the gas product stream to an infrared detector, where methane content was continuously measured, and a gas chromatograph where total gas composition was determined.

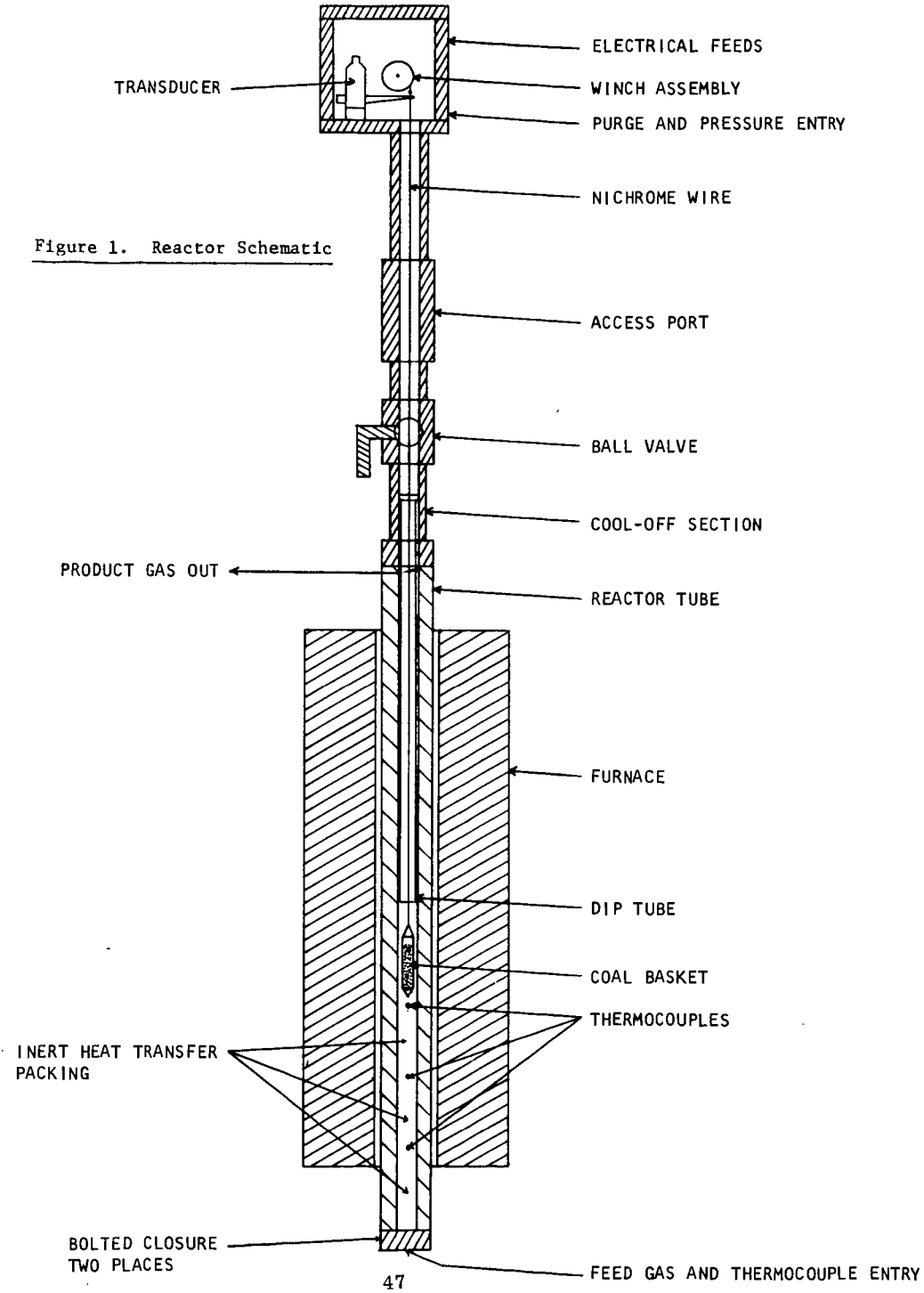

Figure 1. Reactor Schematic

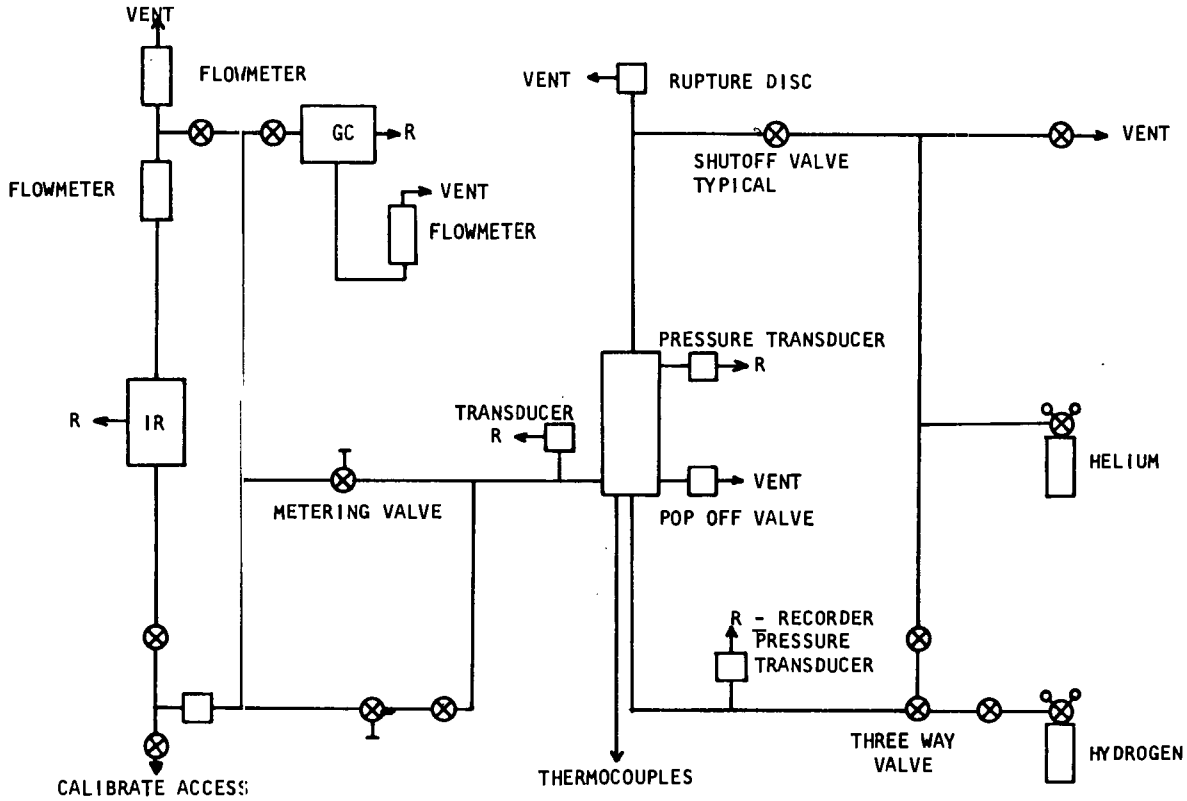

FIGURE 2: SCHEMATIC OF COAL GASIFICATION SYSTEM

All experiments used chars supplied by the Institute of Gas Technology. Char A was a hydrogasified Pittsburgh Seam, Ireland Mine Bituminous coal. Char B was from the same source, but was pre-oxidized (about 1 ft^3 of oxygen per pound of fresh coal at 400°C) in an air fluidized bed. An analysis of the two chars is shown in Table I. The char was sized 18 x 35 mesh sieve fraction, U. S. Standard. The sample weight in any given run was 1.5 - 2.5 grams. The sample bucket was constructed of 100 mesh stainless steel screen.

Catalysts were deposited on the char particles by evaporation from solution. Catalysts concentrations were five percent by weight metal. Catalyst distribution on the char was examined by electron microprobe and scanning electron microscopy.

TABLE I

CHEMICAL ANALYSIS

	Char A (hydrogasified)	Char B (pre-oxidized)
	Uncatalyzed (mass percent)	
Carbon	81.45	67.86
Hydrogen	14.60	3.39
Oxygen	3.76	13.63
Total	99.81	84.88
Volatile	4.61	24.40
Ash	13.94	9.28
	$KHCO_3$ Catalyzed (mass percent)	
Carbon	61.45	55.21
Hydrogen	1.38	3.13
Oxygen	4.57	3.80
Total	67.40	62.14
Volatile	4.60	20.42
Ash	27.29	18.53

III. RESULTS AND DISCUSSION

Reaction of Non-Catalyzed Chars

Initial runs were performed on both chars to determine non-catalyzed reaction rates. Percent of carbon gasified versus time cruves are shown in Figures 3 and 4 for chars A and B, respectively, at 500 and 1000 psi, 950°C. Characteristically, the mass loss curves show high initial reaction rates as the more volatile matter in the char is gasified, followed by a much slower reaction regime where the rate slowly diminishes as the char is consumed. Such phenomena have been previously described by a number of investigators[7-11].

For kinetic analysis of the mass loss data, we propose a model different from those previously discussed. We assume that the reaction rate is given by the following kinetic expression:

$$\frac{dX}{dt} = v_n \, p_{H_2}^n \, (1 - X) \exp \left[- \Delta H^{\neq} / RT \right] \qquad (1)$$

where X = fractional conversion of carbon

v_n = frequency factor

n = order of reaction

$\Delta H^{\neq}$ = activation enthalpy for gasification.

In contrast to homogeneous reactions, where activation enthalpies are independent of extent of reaction, hydrogasification activation enthalpies are clearly a function of extent of reaction. One mechanism, postulated by a number of investigators, is based on the carbon structure becoming more graphitic with increasing extent

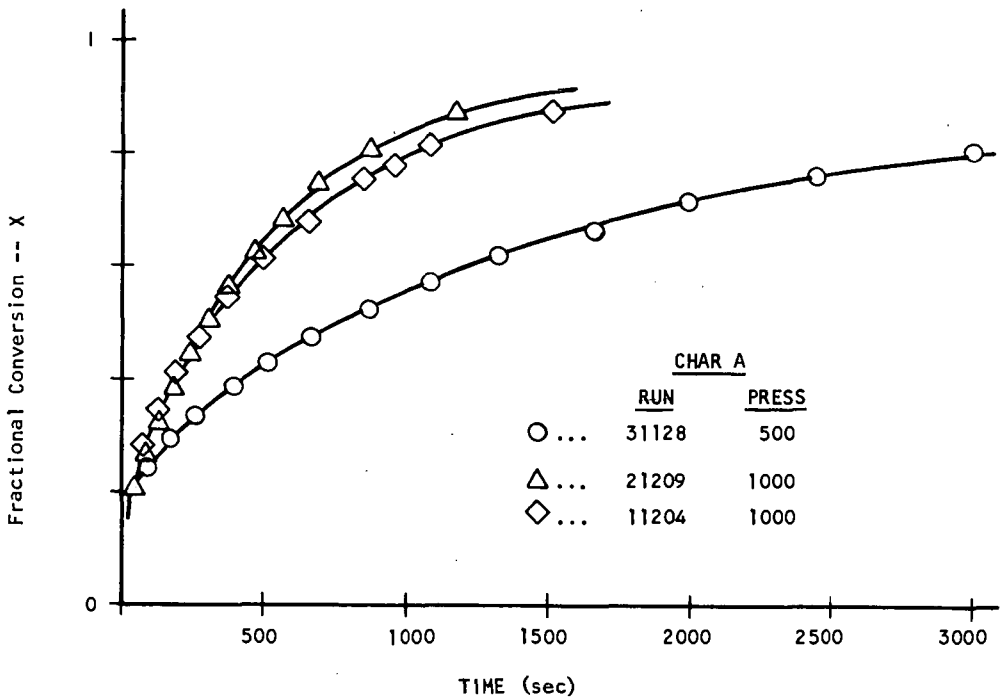

FIGURE 3. NON-CATALYZED HYDROGASIFICATION OF CHAR A AT 500 and 1000 psi, 950°C

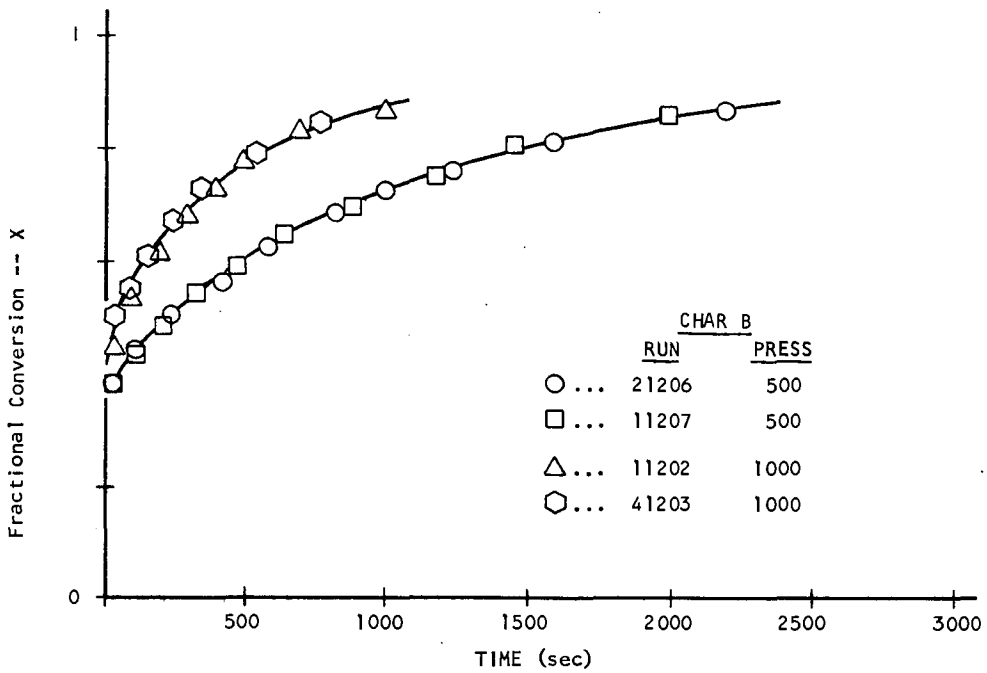

FIGURE 4. NON-CATALYZED HYDROGASIFICATION OF CHAR B AT 500 and 1000 psi, 950°C

of reaction. In the absence of any other information, the simplist function for $\Delta H^{\neq}$ (X) is a linear form

$$\Delta H^{\neq} (X) = \Delta H^0 + \alpha X \qquad (2)$$

where

ΔH^0 = initial activation enthalpy

α = factor that determines sensitivity of $\Delta H^{\neq}$ to X.

Substituting this expression into equation (1), yields

$$\frac{dX}{dt} = kP_{H_2}^n (1 - X) \exp(- \Delta H^0/RT) \exp(- \alpha X/RT) . \qquad (3)$$

By lumping the pressure and temperature terms into two constants, Equation (3) can be written in a simpler form in order to test its applicability as a rate expression. Thus,

$$\frac{dX}{dt} = kP_{H_2}^n \exp(- \Delta H^0/RT) \cdot \exp(\frac{-\alpha}{RT} \cdot X) \cdot (1 - X)$$

and then

$$\frac{dX}{dt} = K \exp(- bX) \cdot (1 - X) \qquad (4)$$

where K and b are both constants and equal to

$$K = kP_{H_2}^n \exp (- \Delta H^0/RT)$$

$$b = \alpha/RT$$

Rearrangement and integration of equation (4) gives the final form of the rate expression used to test the kinetic data.

$$\int_o^X \frac{\exp(bX)}{(1 - X)} dX = \int_o^t Kdt = Kt \qquad (5)$$

Figures 5 and 6 show plots of the integral on the left side of equation (5) versus time for chars A and B, respectively. The parameter b is chosen to minimize the sum of the squares of the

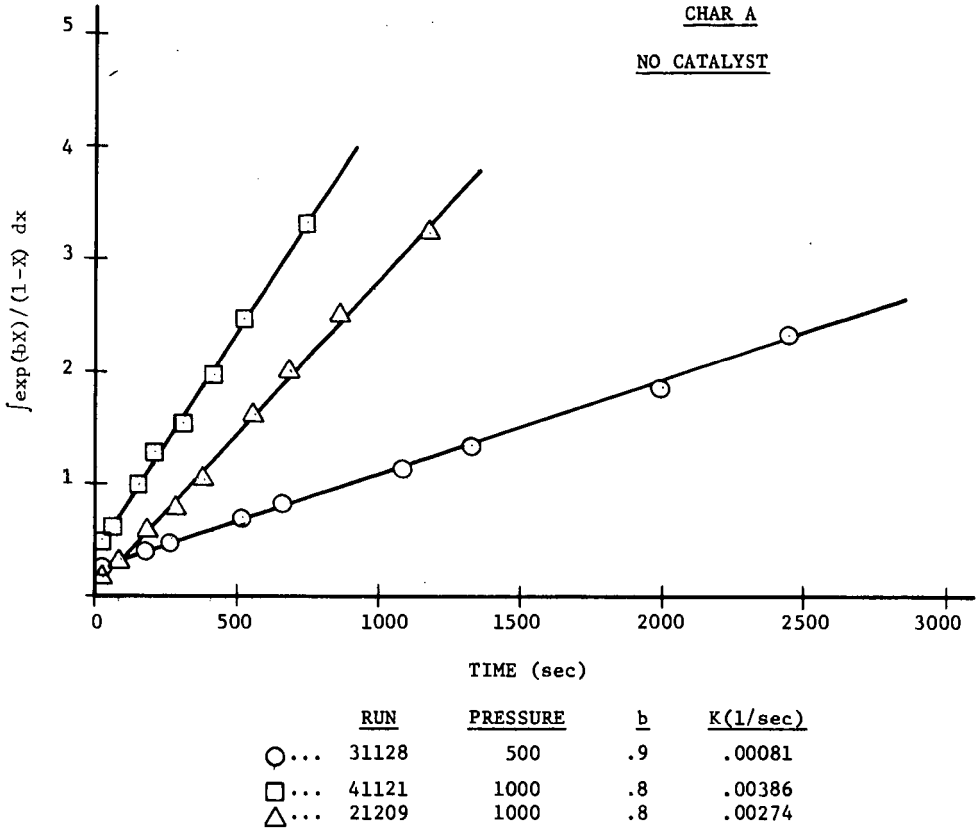

	RUN	PRESSURE	b	K(1/sec)
○...	31128	500	.9	.00081
□...	41121	1000	.8	.00386
△...	21209	1000	.8	.00274

Figure 5. Kinetic Test for the Non-Catalyzed Hydrogasification of Char A at 500 and 1000 psi, 950°C.

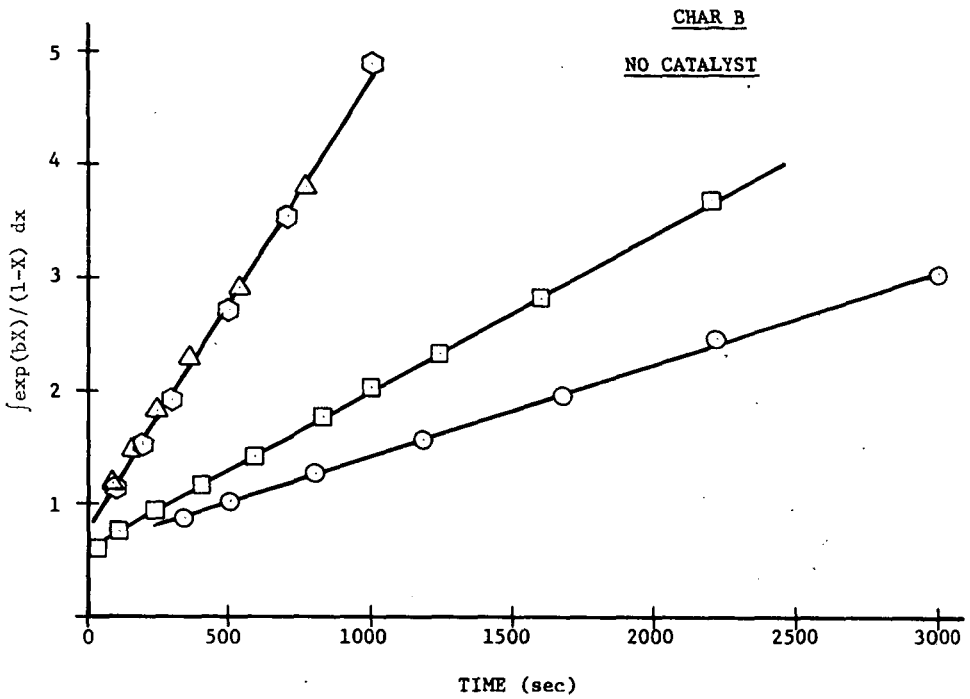

	RUN	PRESS	b	K(1/sec)
○ ...	11124	500	1	.000818
□ ...	21206	500	1	.00143
△ ...	41203	1000	1.2	.00386
⬡ ...	11127	1000	0.9	.00399

Figure 6. Kinetic Test for the Non-Catalyzed Hydrogasification of Char B at 500 and 1000 psi, 950°C.

errors of a least square fit to a straight line through the data points. The value of K is then evaluated from the slope of the straight line.

Table II shows the values of b and K determined from Figures 5 and 6.

The values of b are seen to be independent of the hydrogen pressure within experimental error. The ratio of the K values at 1000 and 500 psi, respectively, are for char A, $K_{1000}/K_{500} = 3.27$ and for char B, $K_{1000}/K_{500} = 2.89$. The hydrogen pressure appears in the K term raised to the power n, where n is the order of the reaction. Thus, the hydrogasification reaction order is approximately 1.6 in hydrogen pressure.

The y-axis intercept in Figures 5 and 6 should have been zero. The positive non-zero intercept results from the very rapid first stage of the hydrogasification reaction. For the pre-oxidized char B, the amount of carbon gasified in the rapid first stage of the reaction is greater than that for the hydrogasified char. This effect is due to the pretreatment of the char. In the second, slower part of the reaction, however, the chars behaved almost identically as indicated by similarity in the values of b and K.

Figure 7 shows the fraction of carbon gasified as a function of time for char B at 850 and 950°C, 1000 psi. The values of K and b at 850°C were found to be 2.3 and .00128 sec^{-1}, respectively. From the variation of K with temperature, the value of ΔH^0 can be estimated to be 29.3 kcal/mole. The activation enthalpy is then given by

TABLE II

TABULATION OF b AND K VALUES FOR
NON-CATALYZED CHAR A AND B

Char A (hydrogasified)					
	500 psi H_2			1000 psi H_2	
Run	b	K	Run	b	K
11122	0.25	0.000974	41121	0.8	0.00386
31128	0.9	0.000810	21209	0.8	0.00274
Average	0.57	0.000892	11204	0.8	0.00212
			Average	0.8	0.00291

Char B (pre-oxidized)					
	500 psi H_2			1000 psi H_2	
Run	b	K	Run	b	K
11124	1	0.000818	11127	0.9	0.00399
21206	1	0.00143	31209	0.8	0.00290
11207	1	0.00147	41203	1.2	0.00386
31207	0.5	0.00125	11202	1.2	0.00406
Average	0.88	0.00124	Average	1.025	0.00372

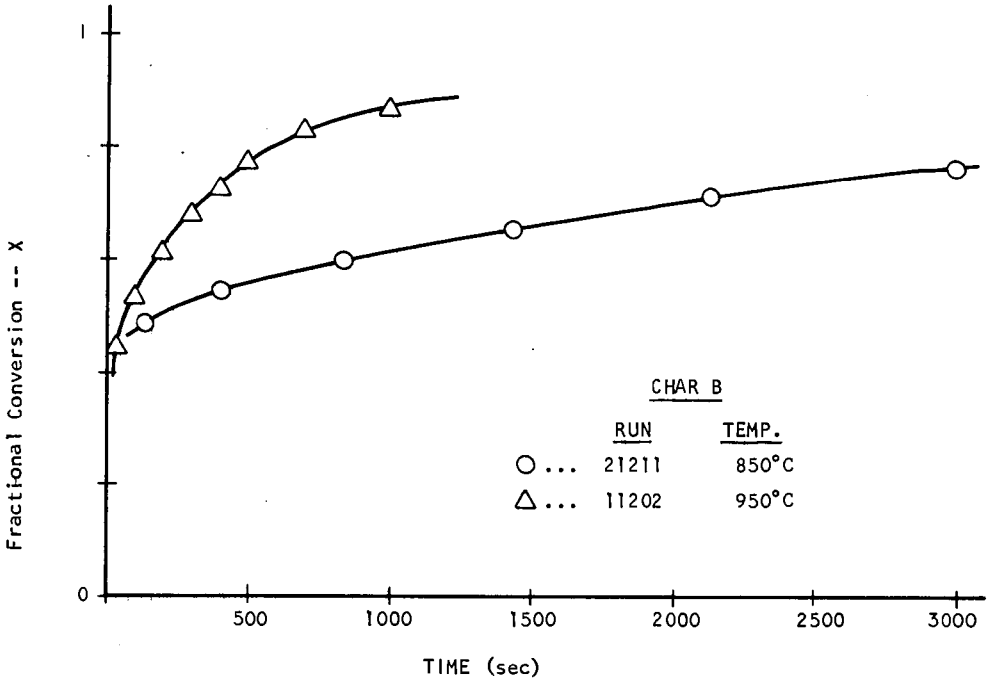

FIGURE 7. EFFECT OF TEMPERATURE ON THE NON-CATALYZED HYDRO-GASIFICATION OF CHAR B AT 850 and 950°C, 1000 psi

the expression,

$$\Delta H^{\neq} \frac{kcal}{mole} = 29.3 + 2.43\ X \qquad (6)$$

for an uncatalyzed char system.

Figure 8 shows a representative composite plot of the carbon fraction converted, the methane rate of production, and the temperature versus time for char B, Run 11128. The concentration of methane in the product stream is proportional to the rate of the hydrogasification reaction, as

$$r = \frac{dP_{CH_4}}{dt} = \frac{1}{12}\frac{1}{n_c}\left(\frac{dV}{dt}\right)\frac{P_{CH_4}}{RT} \qquad (7)$$

where r = rate (moles/minute/initial gms. of carbon)

n_c = initial moles carbon

P_{CH_4} = partial pressure CH_4 in atms

R = gas constant in L - atm/M - °K

T = temperature, °K

$\left(\frac{dV}{dt}\right)$ = product gas flow rate in liters/minute.

Equation (7) can be integrated numerically. The result is shown in Figure 9.

Although the infrared measurement of methane production leads to qualitative agreement with the direct mass determination, quantitative agreement is not good. This is most probably due to axial dispersion in the gas product stream, which results in a loss of kinetic information, and difficulties in precisely regulating the product stream flow rate, which would lead to cumulative errors.

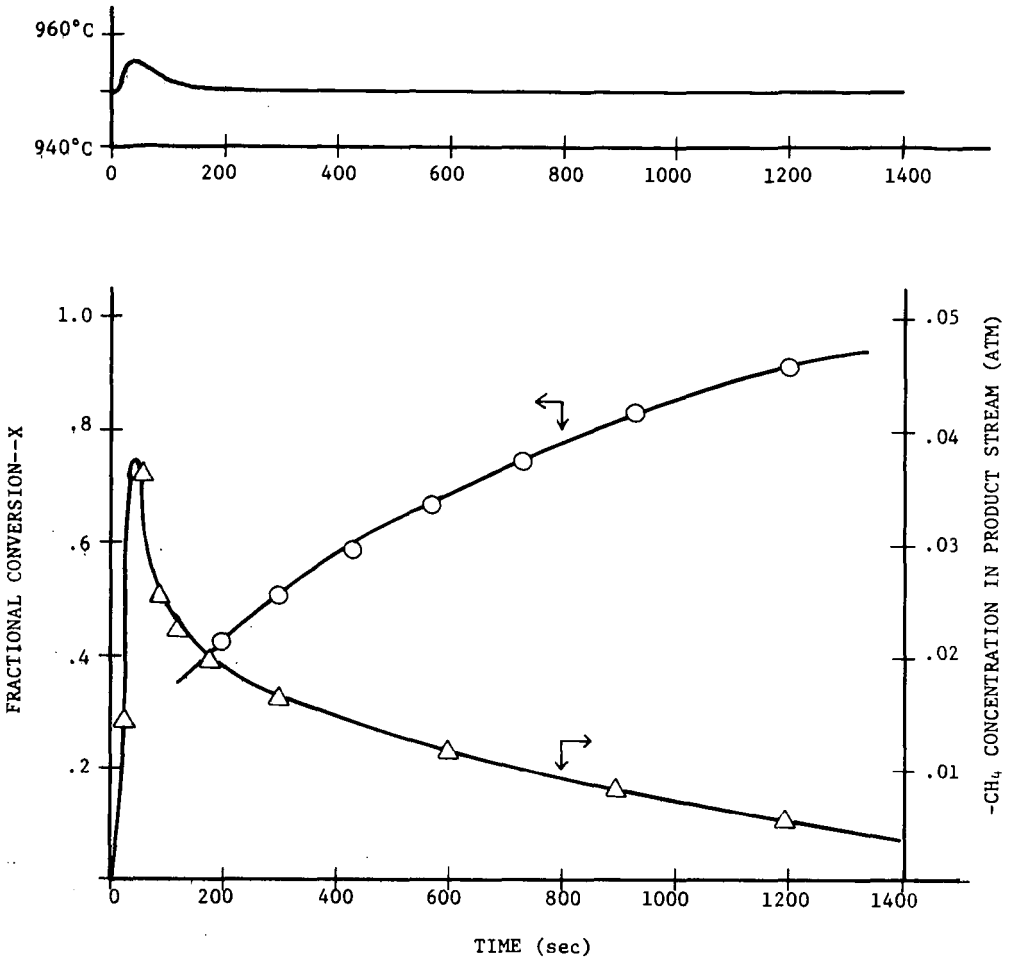

Figure 8. Composite Plot of Rate Data for $KHCO_3$ Catalyzed Char B, Run 11128, at 500 psi and 950°C.

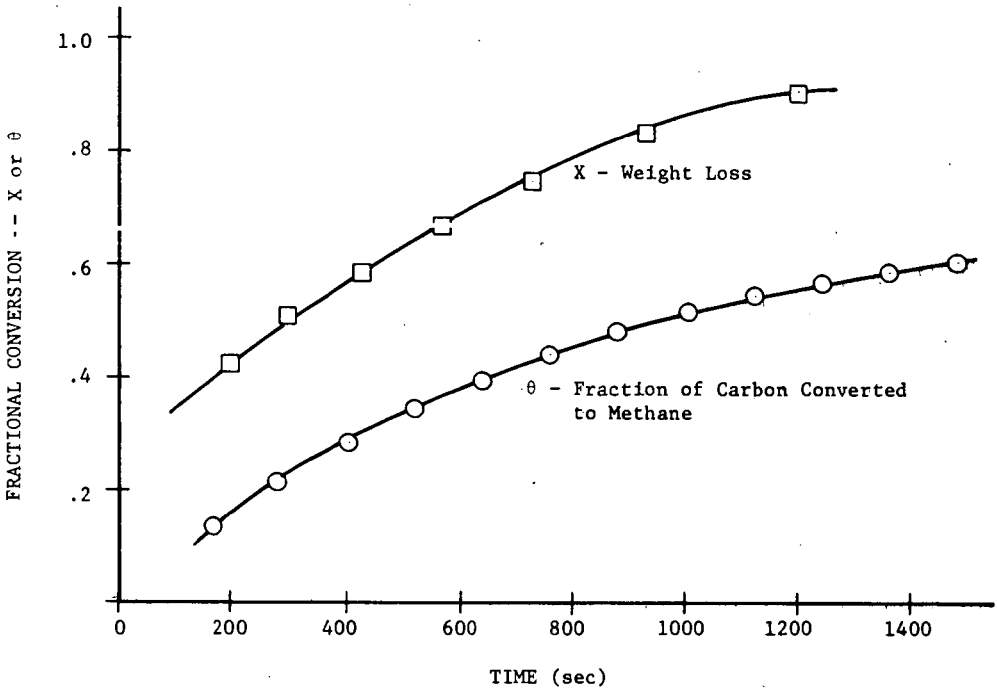

Figure 9. Fractional Conversion of Carbon to Methane for $KHCO_3$ Catalyzed Char A at 500 psi, 950°C.

The temperature versus time curve shown in Figure 8 indicates a small temperature increase resulting from the exothermic hydrogasification reaction, which diminishes with time. Unfortunately, the actual temperature of the char has not been measured directly.

Reaction of Catalyzed Chars

In this preliminary study we have concentrated on catalysts that have long been known to accelerate the hydrogasification reaction, the alkali metals and zinc salts[5]. Figures 10 and 11 show the percent carbon gasified versus time data for a $KHCO_3$ catalyst deposited on chars A and B, respectively, at 950°C, 500 and 1000 psi. Figures 12 and 13 show a representative comparison between the carbon converted in catalyzed and non-catalyzed runs on chars A and B, respectively, at 500 psi and 950°C. A substantial catalytic effect is observed. The time to achieve a gasification fraction X is roughly halved by the $KHCO_3$ catalyst. The kinetic analysis for the parameters b and K are shown in Figures 14 and 15. The kinetic equation (4) is seen to fit the data at high conversions. The evaluation of the b and K parameters for $KHCO_3$ catalyzed reactions is shown in Table III.

The rate enhancement due to the catalysts is shown by the evaluation of α from the parameter b. Taking -1 to be the average value of b for a catalyzed system, the corresponding value of α is -2.43. This term makes the linear expression for the activation enthalpy decrease with increasing carbon gasification

$$\Delta H^{\neq} \text{ (kcal/mole)} = 29.3 - 2.43\ X\ .$$

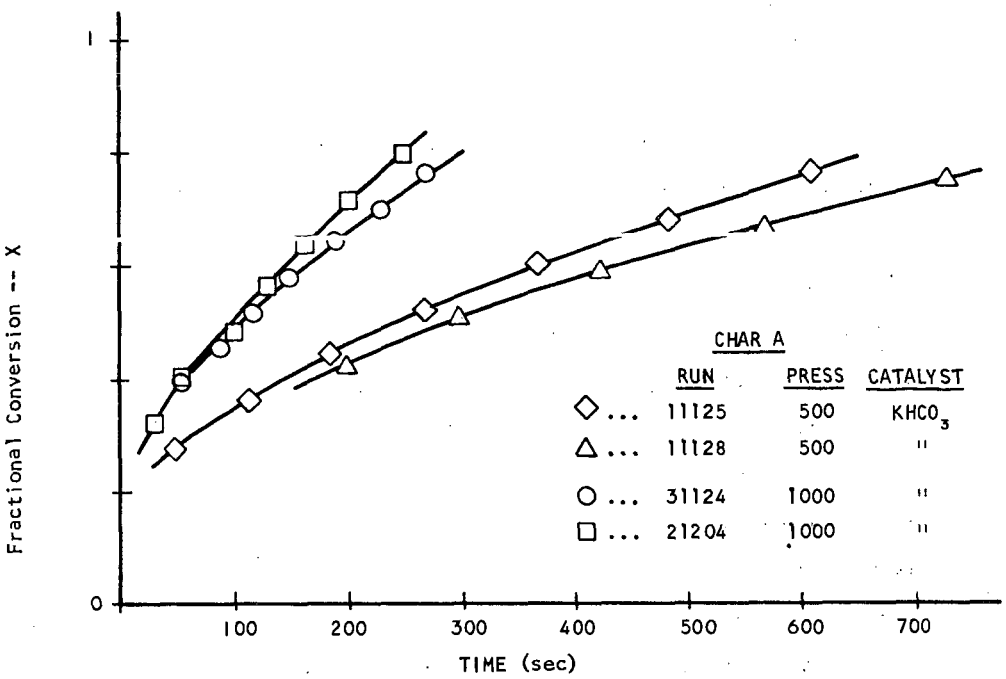

FIGURE 10. CATALYZED HYDROGASIFICATION OF CHAR A AT 500 and 1000 psi, 950°C

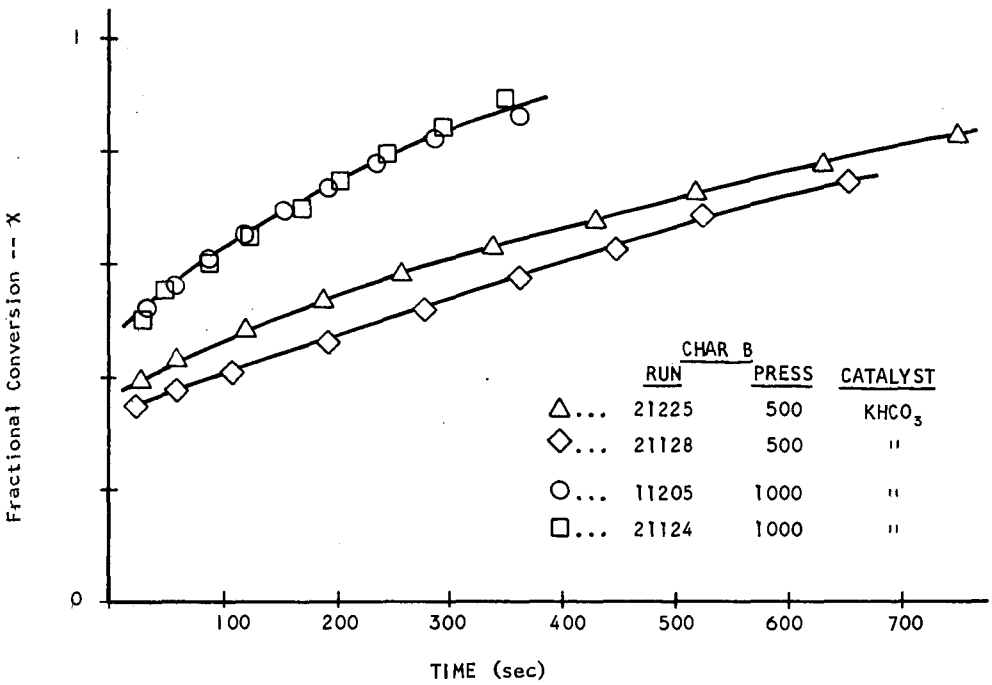

FIGURE 11. CATALYZED HYDROGASIFICATION OF CHAR B AT 500 and 1000 psi, 950°C

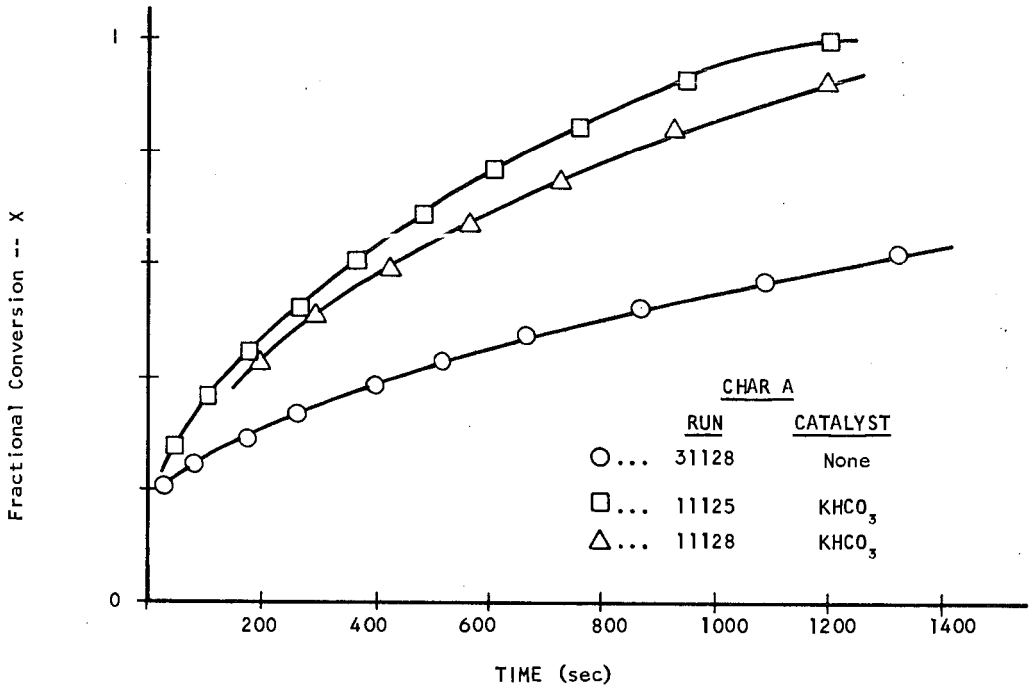

FIGURE 12. COMPARISON OF THE CATALYZED AND NON-CATALYZED HYDROGASIFICATION OF CHAR A AT 500 psi, 950°C

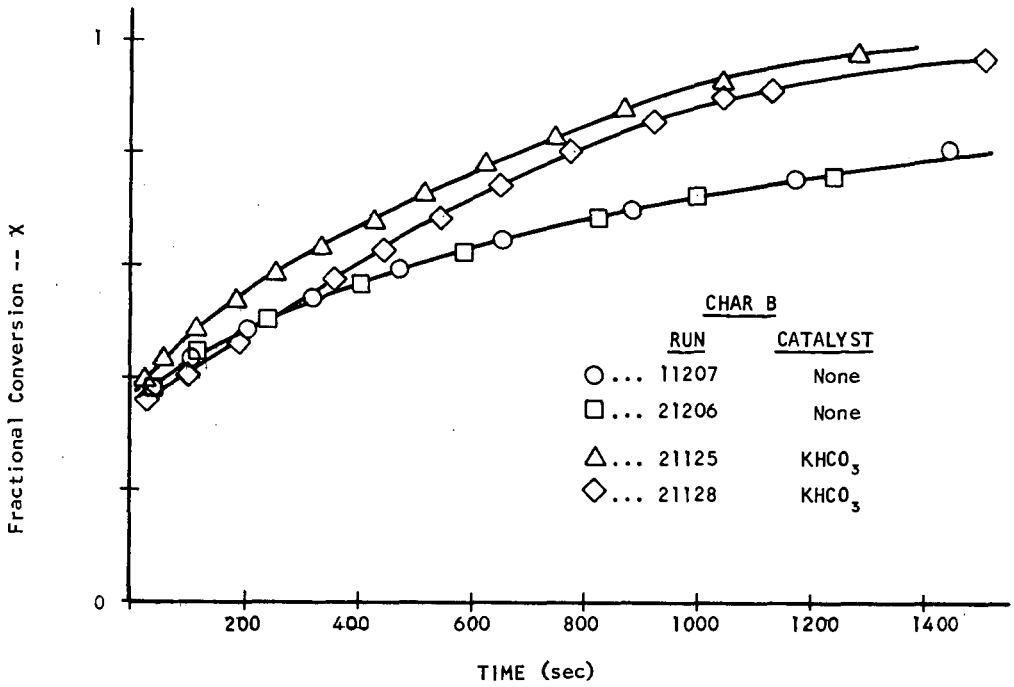

FIGURE 13. COMPARISON OF THE CATALYZED AND NON-CATALYZED HYDROGASIFICATION OF CHAR B AT 500 psi, 950°C

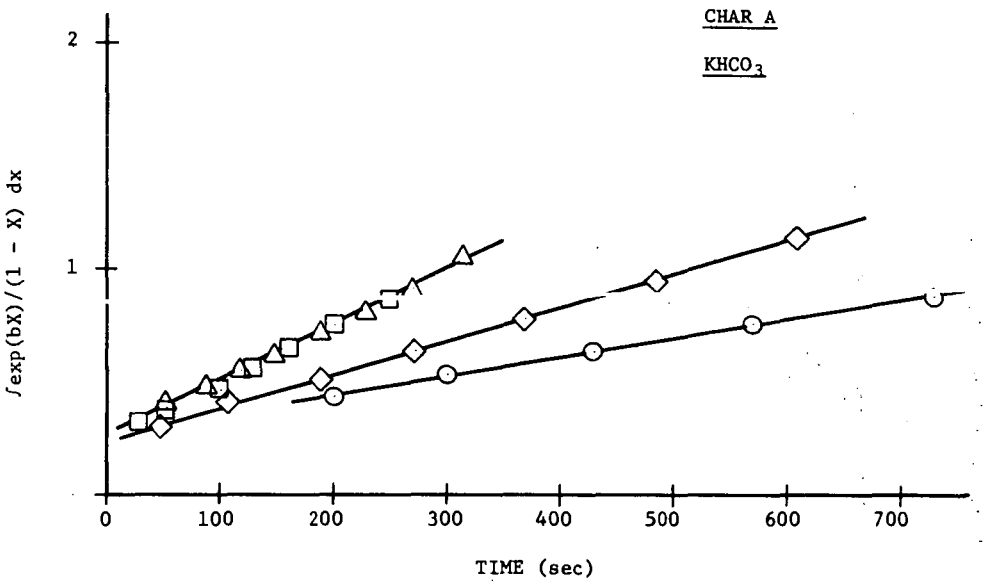

	RUN	PRESSURE	b	K(1/sec)
○...	11128	500	-1.0	.000877
◇...	11125	500	-0.5	.00150
△...	31124	1000	-1.0	.00236
□...	21204	1000	-1.3	.00252

Figure 14. Kinetic Test for the $KHCO_3$ Catalyzed Hydrogasification of Char A at 500 and 1000 psi, 950°C.

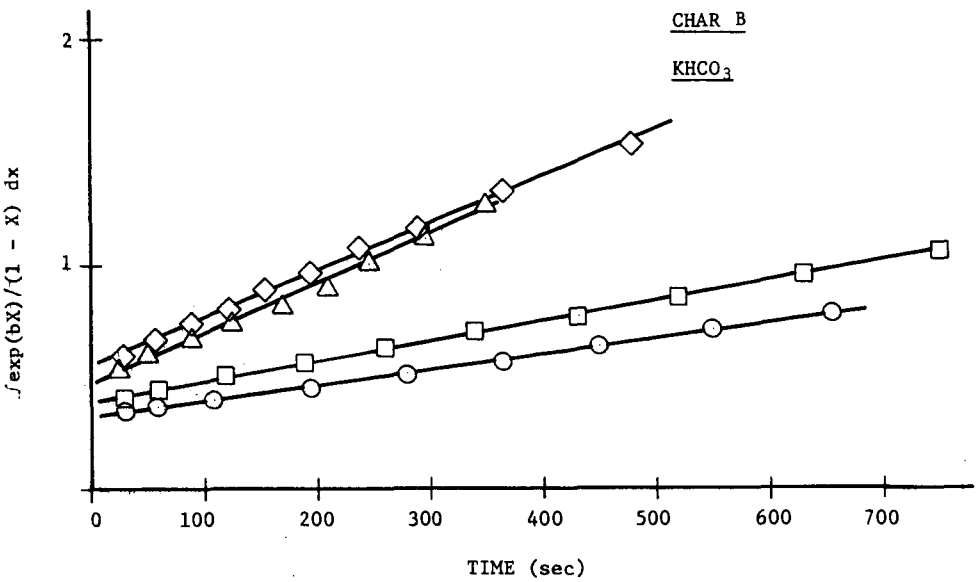

	RUN	PRESSURE	b	K(1/sec)
○ ...	21128	500	-1.3	.000712
□ ...	21125	500	-1.0	.000903
△ ...	21124	1000	-1.0	.00218
◇ ...	11205	1000	-0.75	.00221

Figure 15. Kinetic Test for the $KHCO_3$ Catalyzed Hydrogasification of Char B at 500 and 1000 psi, 950°C.

TABLE III

TABULATION OF b AND K VALUES FOR
CHAR A AND B CATALYZED WITH $KHCO_3$

Char A (hydrogasified)

500 psi H_2			1000 psi H_2		
Run	b	K	Run	b	K
11128	-1.0	0.000877	11208	-0.3	0.00224
11125	-0.5	0.0015	21204	-1.3	0.00252
Average	-0.75	0.00119	31124	-1.0	0.00236
			Average	-0.867	0.00237

Char B (pre-oxidized)

500 psi H_2			1000 psi H_2		
Run	b	K	Run	b	K
21128	-1.3	0.000712	21124	-1.0	0.00218
21125	-1.0	0.000903	11205	-0.75	0.00221
Average	-1.15	0.000807	Average	-0.88	0.00219

Work has also begun on the catalysts potassium carbonate, K_2CO_3, and zinc chloride, $ZnCl_2$. These catalysts were also deposited by impregnation at a five percent by weight metal concentration. The K_2CO_3 catalyst behaved very similar to the $KHCO_3$. The weight loss curves for this catalyst at 500 and 1000 psi, 950°C are shown in Figure 16. Kinetic analysis of this catalyst produced values of b and K similar to those for $KHCO_3$ (see Table IV).

Microscopy of the Chars

Characterization of the chars is being carried out on the microprobe analyzer and the scanning electron microscope. Features such as particle structure, catalyst distribution, and structural change at the catalyst sites during reaction are of interest.

The scanning electron microscope can take high magnification, high resolution pictures of the char particles, while the microprobe analyzer can be calibrated to scan for any element on the char particle surface.

Presented here will be a cross section of representative photos for each char. Proper interpretation of these pictures is important. The scanning micrographs (scanning electron micrographs) are high quality pictures but are often slightly distorted at low magnification (75-100X). The back scattering electron micrographs (BSE) and x-ray micrographs are all taken on the microprobe analyzer. The BSE micrographs from this instrument are of low clarity because the microprobe was designed to do x-ray analysis. An x-ray micrograph is a scattering of white dots on the picture. If the element

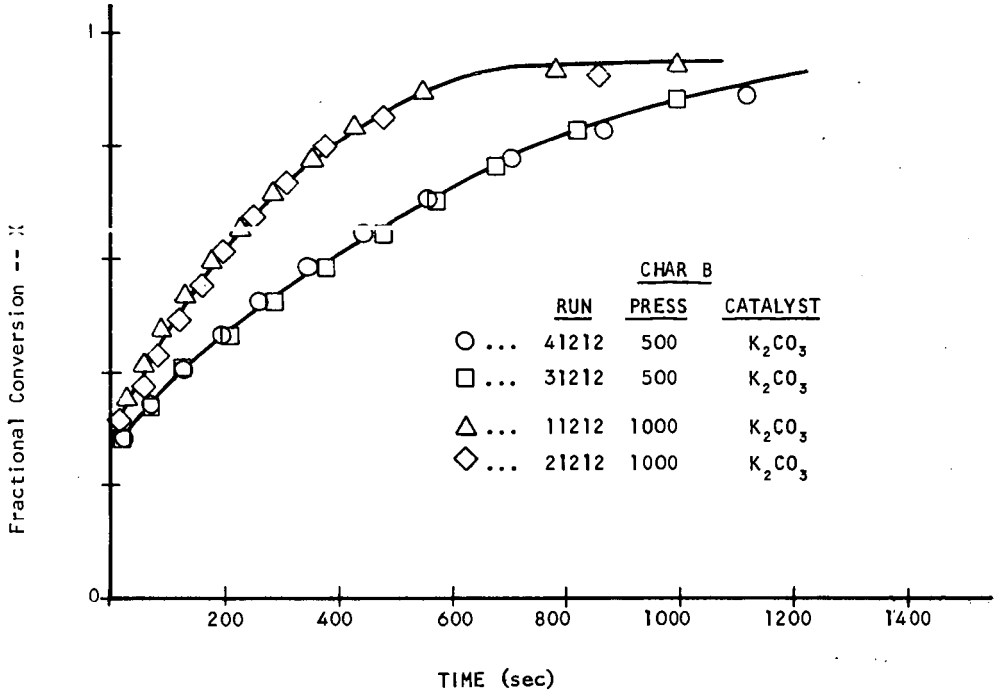

FIGURE 16. CATALYZED HYDROGASIFICATION OF CHAR B AT 500 and 1000 psi, 950°C

TABLE IV

TABULATION OF b AND K VALUES FOR CHAR A AND B
CATALYZED WITH OTHER CATALYSTS

Char A (hydrogasified - $ZnCl_2$)					
	500 psi H_2			1000 psi H_2	
Run	b	K	Run	b	K
21214	0.5	0.00160	21208	0.5	0.00492
31214	0.25	0.00140	51208	0.2	0.00301
Average	0.37	0.00150	Average	0.35	0.00397
Char B (pre-oxidized - K_2CO_3)					
	500 psi H_2			1000 psi H_2	
Run	b	K	Run	b	K
41212	-0.15	0.00155	21212	-0.5	0.00245
31212	-1.2	0.000867	11212	-0.5	0.00248
Average	-0.67	0.00118	Average	-0.5	0.00247

being analyzed is not present, there is an even, but sparce distribution of white dots on the micrograph. (See upper right of Figure 20d where there is no iron present.) This artifact of the analyzer will be referred to as background. The locations where the element being analyzed is present, are then represented by a concentration of white dots. (See also Figure 20d.)

Figure 17a shows a low magnification scanning micrograph of the hydrogasified, $KHCO_3$ catalyzed char A. This is a representative picture of this type of a char, catalyzed or uncatalyzed. The particle surface is, in general, crumpled but smooth.

Higher magnification micrographs of the center of this particle are shown in Figures 17b and 17c. (See the area circled in Figure 17a.) These are both of the same area on the particle. Figure 17b is a scanning micrograph while 17c is a BSE micrograph. Figure 17d is the iron x-ray superimposed on the BSE of Figure 17c. This shows areas of the particle surface where iron deposits or ash concentrations are located. A close-up of the ash deposit circled in Figure 17b or 17c is shown in Figure 18a.

Figure 18b shows a potassium x-ray superimposed on the BSE of Figure 17c, which is $KHCO_3$ catalyzed char A. The heavy but even concentration of white dots indicates that the catalyst is present in a well-distributed manner. The catalyst must exist on the particle surface in a finely divided state since there are no distinguishable clumps, as noticed in earlier catalytic x-ray analysis.

a. Scanning - 75X

b. Scanning - 300X

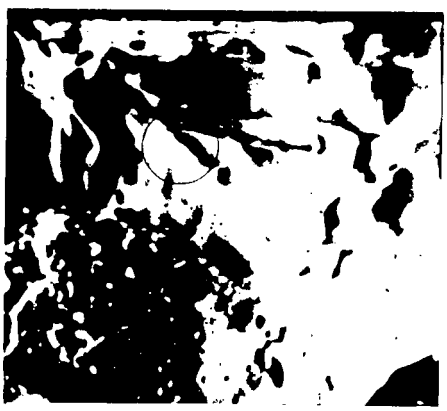

c. BSE - 200X

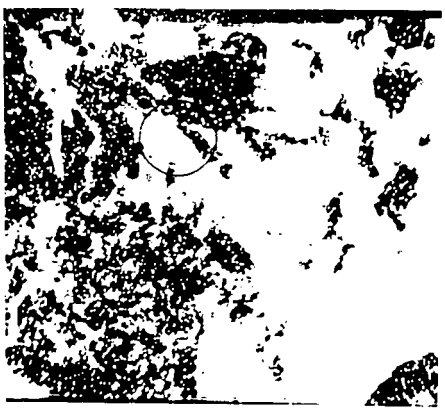

d. Iron X-ray on BSE - 200X

Figure 17. Micrographs of $KHCO_3$ Catalyzed Char A

a. Scanning - 2000X

b. Potassium X-ray on BSE - 200X

c. Cut Particle - Scanning - 100X

d. Cut Particle, Potassium X-ray on BSE - 200X

Figure 18. Micrographs of $KHCO_3$ Catalyzed Char A

The scanning micrograph of a cut particle of char A similar to that in Figure 17a is shown in Figure 18c. The inside of the particle is filled with cavities or cells, somewhat like a sponge. This is very different from the outer surface of the particle. The pretreatment skin[12], or outer surface, and the resulting inner structure are a direct result of the pretreatment history of the char. A potassium x-ray on a BSE micrograph of the area circled in Figure 18c is shown in Figure 18d. This too shows a heavy catalyst concentration.

The pre-oxidized, uncatalyzed or catalyzed char B appears very similar to char A. Direct comparisons of the same type of outer and inner structure can be drawn from Figure 19a and 19b for char B and Figure 17a and 18c for char A. These are the same chars but have undergone different pretreatment histories.

Direct similarities of ash content can be shown with the scanning micrographs of a particle reacted in hydrogen for eight minutes. Figure 20a and 20b show a portion of an uncatalyzed particle with the close-up of an ash deposit in Figure 20b. This can be verified with the results of Figure 20c and 20d, which are the iron x-ray and BSE micrographs of the same area in Figure 20a. In these same areas lighter concentrations of potassium and silicon have also been found.

The analysis of the $KHCO_3$ catalyzed char B showed a good distribution, which was similar to that of char A. (See Figure 18b for char A.)

a. Cut Particle, Scanning - 75X

b. Whole Particle, Scanning - 200X

Figure 19. Micrographs of Uncatalyzed Char B

a. SEM - 500X

b. SEM - 2000X

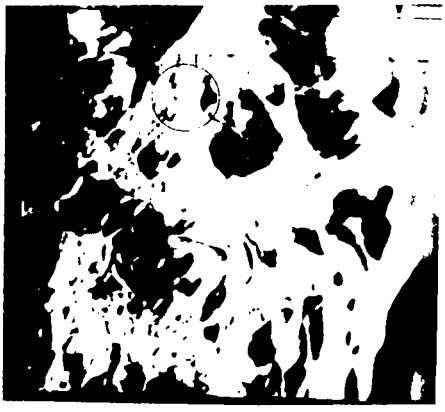

c. BSE - 200X

d. Iron X-ray - 200X

Figure 20. Micrographs of Uncatalyzed Char B

The high iron content is a common characteristic of the two chars and is seen in the x-ray analysis. These chars also have a high sulfur content, which is distributed fairly evenly in the particles. Analysis for zinc and nickel were negative, and slight traces of calcium have been seen in some samples.

IV. CONCLUSIONS

The initial studies of catalysts and contacting systems has begun at Case Western Reserve University. The high temperature, high pressure, recording thermobalance has made direct kinetic analysis of the carbon weight loss curves straightforward.

The data seems to be well represented by the kinetic model proposed in equation (5). Analysis of the fitting parameters for this model show that for the rate dependence on pressure the order of the reaction is about 1.6.

The temperature dependence of the rate constant determines the initial activation enthalpy. The initial activation enthalpy is about 29.3 kcal/mole. Coupling this with the evaluation of the parameter b from the kinetic model we have found the linear form of the activation enthalpy as a function of conversion for a non-catalyzed char. (See equation (6).)

Some information of the relative volatilities of the two chars is discernable from the y-axis intercept in the plots of the kinetic test for our rate expression. This is the portion of the weight loss curves where the rapid first stage of the reaction is taking place. The application of the kinetic model then precedes from the latter part of these curves, which represent the second, slower part of the reaction. Unfortunately, this semi-empirical model leaves us with the lack of a real mechanism. Possibilities of

ash diffusion and/or chemical effects have not been studied in the detail necessary to shed light upon the subject.

The catalytic systems showed substantial slope increases in the weight loss curves (Figure 21). It was found that $KHCO_3$ and K_2CO_3 exhibited an equivalent catalytic effect which was better than that found for $ZnCl_2$ (see values of b in Table IV). The net result of the catalytic systems on our kinetic model was to change the value of the parameter b, which changed the value of α in the linear expression for the activation enthalpy. For the $KHCO_3$ system the value of α for an average value of $b = -.91$ was $\alpha = -2.21$. The catalyst apparently did not affect the value of ΔH° over the course of the reaction.

Microscopy of the char samples is yielding interesting and qualitative information. Characterization of char structure with the scanning electron microscopy has shown the standard pretreatment skin and the celled particle interior. X-ray analysis of the same particles in the microprobe analyzer and the SEM have shown ash deposits on the surface of the char and good catalyst distributions.

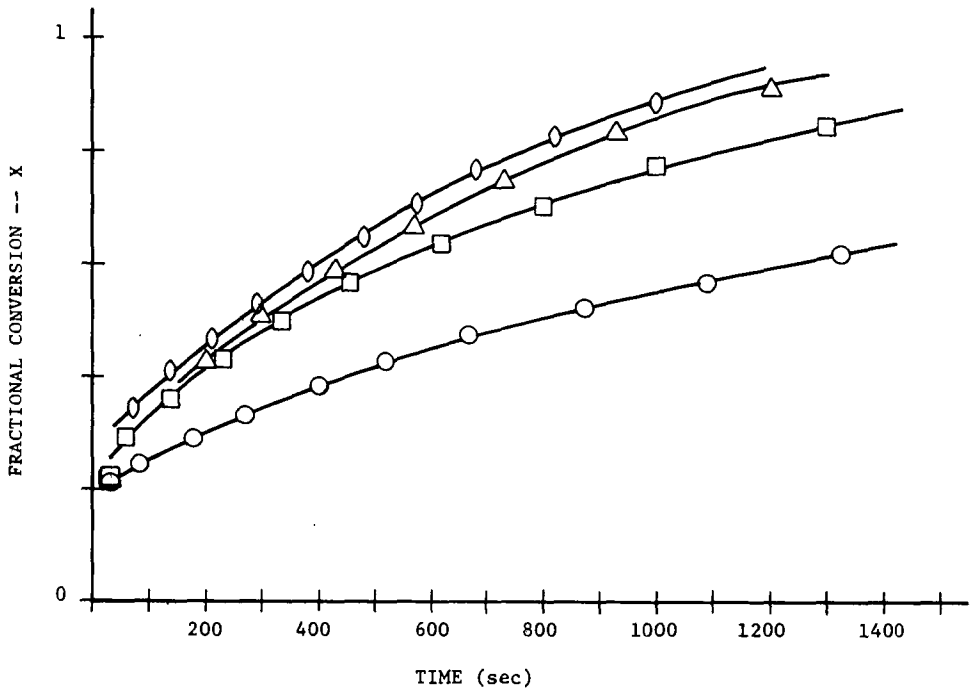

	Run	Char	Catalyst
○ ...	31128	A	none
□ ...	21124	A	$ZnCl_2$
△ ...	11128	A	$KHCO_3$
◊ ...	31212	B	K_2CO_3

Figure 21. Comparison of Various Char-Catalyst Systems at 950°C and 500 psi.

REFERENCES

(1) Dent, F. J., Blackburn, W. M., and Millett, H. C., Trans. Inst. Gas Engrs., 87, 231 (1937)

(2) Friedman, S., Kaufman, M. L., and Wender, I., J. Org. Chem., 36, 694 (1971)

(3) Weller, S., and Pelipetz, M. G., Ind. & Eng. Chem., 43, 1243 (1951)

(4) Dent, F. J., Blackburn, W. H., and Millett, H. C., Trans. Inst. Gas Engrs., 88, 150 (1938)

(5) Wood, R. E., and Hill, G. R., ACS Division of Fuel Chemistry, Vol. 17, No. 1, Aug. 1972

(6) Feldkirchner, H. L., and Johnson, J. J., Rev. Sci. Instr., 39, No. 8, 1227, Aug. 1968

(7) Blackwood, J. D., and McCarthy, D. J., Aust. J. Chem., 19, 797 (1966)

(8) Moseley, F., and Paterson, D., J. Inst. Fuel, 38, 13 (1965)

(9) Feldkirchner, H. L., and Linden, H. R., Industr. Eng. Chem., 2, 153 (1963)

(10) Johnson, J. J., Seminar on Characterization and Characteristics of U.S. Coals for Practical Use, Pennsylvania State University, 1971

(11) Hiteschue, R. W., Friedman, S., and Madden, R., U.S. Bureau of Mines, Reports of Investigation, Nos. 6027 and 6125, 1962

(12) Gould, R. F., Ed., Fuel Gasification, Advances in Chemistry Series, 69, American Chemical Society, 1967

ACKNOWLEDGEMENTS

We gratefully acknowledge the American Gas Association's support under Contract No. BR-75-1.

The thermobalance was made available by Consolidated Natural Gas Service Company, Inc., without which this work would have been impossible.

Special thanks are given to Raymond R. Cwiklinski and Donald C. Grant for their technical assistance.